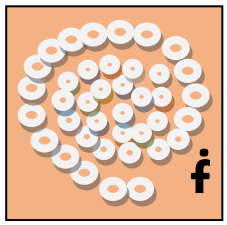

International Journal of Mathematical Analysis and Modelling

(Formerly Journal of the Nigerian Society for Mathematical Biology)

Volume 8 Issue 2, 2025

ISSN (Print): 2682 - 5694
ISSN (Online): 2682 – 5708
www.tnsmb.org

Mathematical modeling and simulation of liquid chromatography for bi-Langmuir isothermal process

M. Uche*, U.D. Uche†‡, and A.I. Anya§

Abstract

A general rate model of liquid chromatography is used to simulate isothermal operating conditions considering the bi-Langmuir isotherm in a cylindrical column. Radial dispersion inside the column are ignored, hence making it a one-dimensional flow problem. The governing equation is composed of a system of partial differential equations together with the nonlinear expression of isotherm and completed with the Danckwerts boundary conditions. A high resolution finite volume scheme of Koren is used to obtain approximate solutions of the governing equation. The scheme is second to third order accurate and easily implemented. Several case studies of single- and multi-components are carried out to study the behaviors of key model parameters. The results show that the suggested finite volume scheme avoids numerical oscillations and provides optimum predictions for the obtained solutions.

Keywords and phrases: liquid chromatography; finite volume scheme; bi-Langmuir isotherm; general rate model

1 Introduction

Liquid chromatography is a technique used for separation of a sample into into its individual parts by relying on the interactions between the sample and the stationary/mobile phases inside the column. The most popular type of liquid chromatography is liquid-solid column chromatography, where a liquid mobile phase filters down through a solid stationary phase, separating components based on their affinity for the mobile phase. This technique has various applications, including in the manufacturing, legal, research, and medical industries [1, 2, 3, 4]. The efficacy of the separation in liquid chromatography is dependent on the polarity of the mobile phase solvent, the nature of the stationary phase, and the composition of the mobile phase [5].

Mathematical modeling can be a valuable tool for designing and optimizing chromatographic methods and for gaining a deeper understanding of the underlying separation mechanisms. Mathematical modeling has been used to predict and optimize separation outcomes based on various parameters such as mobile phase composition and flow rate. Models have been developed to predict chromatographic peak shape and retention time based on the properties of the analyte and the stationary phase [5, 1, 6]. Several of these models describing liquid chromatography process and representing different levels of complexities can be found in the literature [5, 1, 8, 9, 10, 11, 12, 7, 13, 14].

In this article, the analysis in [15] for linear and nonlinear Langmuir isotherm is extended to incorporate the operations considering nonlinear bi-Langmuir isotherm. The contributions of this work include the implementation of the bi-Langmuir isotherm using the general rate model which accounts for both external mass transfer and intra-particle diffusion inside the column; the study of these parameters on how they affect separation for bi-Langmuir isotherm analysis and the extension of the suggested

*Mathematics Programme, National Mathematical Centre Abuja, Nigeria

†Corresponding Author; E-mail: uuche@nmc.edu.ng, duj_uche@yahoo.com; Mathematics Programme, National Mathematical Centre Abuja, Nigeria

‡Department of Mathematics, University of Abuja, Nigeria

§Department of Mathematical Sciences, Veritas University Abuja, Bwari-Abuja, Nigeria

finite volume scheme to obtain approximate solutions for the governing equations of the model. The finite volume scheme has been applied severally in finding numerical approximations to governing model equations of liquid chromatography and is found easily implementable [16, 17, 18, 19, 20, 21]. The current suggested semi-discrete scheme is capable of computing weak solutions of the governing equations and properly captures the narrow peaks of the concentration profiles [22, 16]. Case studies, which cover a the range of key kinetic parameters, are carried out to illustrate and study their effects. The results obtained are useful for further developments in the application of liquid chromatographic processes.

2 The governing equations

Consider an isothermal adsorption column packed with uniform spherical shaped fully-porous particles with radius R_{p} where radial dispersion is neglected. Let t, z and r_{p} represent the time coordinate, axial coordinate and radial coordinate of the spherical particles, respectively. For a constant velocity u through out the length of the column, the classical equation of mass balance in the mobile phase of the fluid for n number of components is given as

$$\frac{\partial c_{\mathrm{i}}}{\partial t} + u\frac{\partial c_{\mathrm{i}}}{\partial z} = D_{\mathrm{i}}\frac{\partial^2 c_{\mathrm{i}}}{\partial z^2} - \frac{3}{R_{\mathrm{p}}}Fk_{\mathrm{i}}\left(c_{\mathrm{i}} - c_{\mathrm{pi}}(r_{\mathrm{p}} = R_{\mathrm{p}})\right), \qquad i = 1, 2, \ldots, n. \tag{1}$$

In the equation above, c_{i} represents the solute concentration in the mobile phase of the fluid for component i, ϵ_b is the external porosity, D_{i} denotes the dispersion coefficient, c_{p} is the solute concentration in the particle pores, k_{i} is the external mass transfer coefficient and $F = \frac{1-\epsilon}{\epsilon}$ is the phase ratio with ϵ defined as the external porosity.

The equation of mass for the solute concentration of n components in the spherical particles pores can be given as

$$\epsilon_{\mathrm{p}}\frac{\partial c_{\mathrm{pi}}}{\partial t} + (1-\epsilon_{\mathrm{p}})\frac{\partial q_{\mathrm{pi}}}{\partial t} = \epsilon_{\mathrm{p}} D_{\mathrm{pi}}\left[\frac{1}{r_{\mathrm{p}^2}}\frac{\partial}{\partial r_{\mathrm{p}}}\left(r_{\mathrm{p}^2}\frac{\partial c_{\mathrm{pi}}}{\partial r_{\mathrm{p}}}\right)\right], \quad i = 1, 2, \ldots, n \tag{2}$$

where, q_{pi} is the local concentration of solute in the shell of the stationary phase, D_{pi} is the pore diffusivity and ϵ_{p} is the internal porosity.

The following dimensionless variables are applied to reduce and simplify the governing model equations:

$$x = \frac{z}{L}, \quad \tau = \frac{ut}{L}, \quad Pe_{\mathrm{i}} = \frac{Lu}{D_{\mathrm{i}}}, \quad \rho_{\mathrm{p}} = \frac{r_{\mathrm{p}}}{R_{\mathrm{p}}}, \quad \zeta_{\mathrm{i}} = \frac{k_{\mathrm{i}}R_{\mathrm{p}}}{D_{\mathrm{pi}}} \quad \eta_{\mathrm{i}} = \frac{D_{\mathrm{pi}}L}{R_{\mathrm{p}^2}u}, \quad \xi_{\mathrm{i}} = 3\zeta_{\mathrm{i}}\eta_{\mathrm{i}}F.$$

Here, L is the characteristic column length, Pe_{i} is the peclet number, ζ_{i} is the Biot number for mass η_{i} and ξi are the dimensionless constants. By applying the above dimensionless variables, the governing model equations now become

$$\frac{\partial c_{\mathrm{i}}}{\partial \tau} + \frac{\partial c_{\mathrm{i}}}{\partial x} = \frac{1}{Pe_{\mathrm{i}}}\frac{\partial^2 c_{\mathrm{i}}}{\partial x^2} - \xi_{\mathrm{i}}\left[c_{\mathrm{i}} - c_{\mathrm{pi}}|_{\rho_{\mathrm{p}}=1}\right], \tag{3}$$

$$\frac{\partial c_{\mathrm{pi}}}{\partial \tau} + (\frac{1-\epsilon_{\mathrm{p}}}{\epsilon_{\mathrm{p}}})\frac{\partial q_{\mathrm{pi}}}{\partial \tau} = \frac{\eta_{\mathrm{i}}}{\rho_{\mathrm{p}^2}}\frac{\partial}{\partial \rho_{\mathrm{p}}}\left(\rho_{\mathrm{p}^2}\frac{\partial c_{\mathrm{pi}}}{\partial \rho_{\mathrm{p}}}\right). \tag{4}$$

The multi-component bi-Langmuir isotherm defined below is applied in this work to describe the interaction between the mobile and stationary phases [1],

$$q_{\mathrm{pi}} = \frac{H_{1\mathrm{i}}c_{\mathrm{pi}}}{1 + \sum_{\mathrm{j}=1}^{n} b_{1\mathrm{j}}c_{\mathrm{pj}}} + \frac{H_{2\mathrm{i}}c_{\mathrm{pi}}}{1 + \sum_{\mathrm{j}=1}^{n} b_{2\mathrm{j}}c_{\mathrm{pj}}}, \quad i = 1, 2, \ldots, n. \tag{5}$$

H_1, H_2 above are the Henry's constants and b_{ij}'s (strictly positive) are the Langmuir factors or coefficients of nonlinearity.

The system of PDEs require the following initial and boundary conditions.

Initial conditions:

$$c_i(x, \tau = 0) = 0, \quad 0 \le x \le 1, \tag{6}$$

$$c_{pi}(\rho_p, x, \tau = 0) = 0, \quad 0 \le \rho_p \le 1, \ \ 0 \le x \le 1. \tag{7}$$

At both column boundaries, the Danckwerts boundary conditions are used for rectangular pulse injection:

$$c_i(x = 0, \tau) - \frac{1}{Pe_i}\frac{\partial c_i(x = 0, \tau)}{\partial x} = \begin{cases} c_i^{inj}, & \text{if } 0 < \tau \le \tau_{inj}, \\ 0, & \tau > \tau_{inj}. \end{cases} \tag{8}$$

where c_i^{inj} is the injected concentration and τ_{inj} is the dimensionless time of injection. At the outlet of the column, the classic Neumann boundary conditions is applied:

$$\left.\frac{\partial c_i(x, \tau)}{\partial x}\right|_{x=1} = 0. \tag{9}$$

Lastly for the particle phase, equation (4), the following boundary conditions are used at $\rho_p = 0$ and $\rho_p = 1$ as

$$\left.\frac{\partial c_{pi}}{\partial \rho_p}\right|_{\rho_p=0} = 0, \quad \left.\frac{\partial c_{pi}}{\partial \rho_p}\right|_{\rho_p=1} = \zeta_i(c_i - c_{pi}|_{\rho_p=1}). \tag{10}$$

3 Numerical approximation

There are various numerical schemes that can be applied either as a combination of two schemes or just a single scheme available in the literature [7, 11, 1, 16, 23]. However, the current suggested scheme is found to be easily implemented and efficiently handles the nonlinearity of the model equations posed by the bi-Langmuir isotherm. The following system of equations are obtained from equations (3) and (4) by using the bi-Langmuir adsorption isotherm described in equation (5) considering two component solutes inside the column. The process is similar for a single solute or more than two component solutes.

$$\frac{\partial \mathbf{c}}{\partial \tau} + \frac{\partial \mathbf{c}}{\partial x} - \mathbf{P}\frac{\partial^2 \mathbf{c}}{\partial x^2} + \xi(\mathbf{c} - \mathbf{c}_p|_{\rho_p=1}) = 0, \tag{11}$$

$$\mathbf{J}\frac{\partial \mathbf{c}_p}{\partial \tau} - \eta\left(\frac{\partial^2 \mathbf{c}_p}{\partial \rho_p^2} + \frac{2}{\rho_p}\frac{\partial \mathbf{c}_p}{\partial \rho_p}\right) = 0, \tag{12}$$

where

$$\mathbf{c} = \begin{bmatrix} c_1 \\ c_2 \end{bmatrix}, \ \mathbf{c}_p = \begin{bmatrix} c_{p1} \\ c_{p2} \end{bmatrix}, \ \mathbf{P} = \begin{bmatrix} \frac{1}{Pe_1} & 0 \\ 0 & \frac{1}{Pe_2} \end{bmatrix}, \ \xi = \begin{bmatrix} \xi_1 & 0 \\ 0 & \xi_2 \end{bmatrix}, \ \eta = \begin{bmatrix} \eta_1 & 0 \\ 0 & \eta_2 \end{bmatrix},$$

$$\mathbf{J} = \begin{bmatrix} \epsilon_p + (1-\epsilon_p)\frac{\partial q_{p1}}{\partial c_{p1}} & (1-\epsilon_p)\frac{\partial q_{p1}}{\partial c_{p2}} \\ (1-\epsilon_p)\frac{\partial q_{p2}}{\partial c_{p1}} & \epsilon_p + (1-\epsilon_p)\frac{\partial q_{p2}}{\partial c_{p2}} \end{bmatrix}.$$

Now, we note that $c := c(x, \tau)$, $c_p := c_p(\rho_p, x, \tau)$ and at any dimensionless time τ, we define

$$(c)_m = (c)_m(\tau) = \frac{1}{\Delta x_m}\int_{I_m} c(x, \tau)dx, \tag{13}$$

$$(c_p)_{mn} = (c_p)_{mn}(\tau) = \frac{1}{\Delta x_m \Delta \rho_{p_n}}\int_{\Omega_{mn}} c(\rho_p, x, \tau)d\rho_p dx. \tag{14}$$

Next we integrate equations (11) and (12) over the intervals $I_{\rm m}$ and $\Omega_{\rm mn}$ respectively to obtain

$$\frac{d(\mathbf{c})_{\rm m}}{d\tau} = -\frac{(\mathbf{c})_{\rm m+\frac{1}{2}} - (\mathbf{c})_{\rm m-\frac{1}{2}}}{\Delta x} + \frac{\mathbf{P}}{\Delta x}\left[\left(\frac{\partial \mathbf{c}}{\partial x}\right)_{\rm m+\frac{1}{2}} - \left(\frac{\partial \mathbf{c}}{\partial x}\right)_{\rm m-\frac{1}{2}}\right] - \xi\left((\mathbf{c})_{\rm m} - (\mathbf{c}_{\rm p})_{\rm mn}|_{\rho_{\rm p}=1}\right), \tag{15}$$

$$\frac{d(\mathbf{c}_{\rm p})_{\rm mn}}{d\tau} = \frac{\mathbf{J}_{\rm mn}^{-1}\eta}{\Delta\rho_{\rm p}}\left[\left(\frac{\partial \mathbf{c}_{\rm p}}{\partial \rho_{\rm p}}\right)_{\rm mn+\frac{1}{2}} - \left(\frac{\partial \mathbf{c}_{\rm p}}{\partial \rho_{\rm p}}\right)_{\rm mn-\frac{1}{2}} + 2\cdot\frac{(\mathbf{c}_{\rm p})_{\rm mn+\frac{1}{2}} - (\mathbf{c}_{\rm p})_{\rm mn-\frac{1}{2}}}{\rho_{\rm pn+\frac{1}{2}}}\right], \tag{16}$$

where $I_{\rm m} \equiv [x_{\rm m-\frac{1}{2}}, x_{\rm m+\frac{1}{2}}]$ and $\Omega_{\rm mn} \equiv [x_{\rm m-\frac{1}{2}}, x_{\rm m+\frac{1}{2}}] \times [\rho_{\rm pn-\frac{1}{2}}, \rho_{\rm pn+\frac{1}{2}}]$ composed of uniform mesh sizes defined on the domain $[0,1]\times[0,1]$, for $1 \le m \le N_x$, $1 \le n \le N_{\rho_{\rm p}}$ and having the coordinate points $(x_{\rm m}, \rho_{\rm pn})$

$$x_{\rm m} = \frac{x_{\rm m-\frac{1}{2}} + x_{\rm m+\frac{1}{2}}}{2}, \qquad \rho_{\rm pn} = \frac{\rho_{\rm pn-\frac{1}{2}} + \rho_{\rm pn+\frac{1}{2}}}{2}.$$

The remaining derivatives in equations (15) and (16) are approximated below as

$$\left(\frac{\partial \mathbf{c}}{\partial x}\right)_{\rm m\pm\frac{1}{2}} = \pm\frac{((\mathbf{c})_{\rm m\pm1} - (\mathbf{c})_{\rm m})}{\Delta x}, \qquad \left(\frac{\partial \mathbf{c}_{\rm p}}{\partial \rho_{\rm p}}\right)_{\rm m,n\pm\frac{1}{2}} = \pm\frac{((\mathbf{c}_{\rm p})_{\rm m,n\pm1} - (\mathbf{c}_{\rm p})_{\rm mn})}{\Delta\rho_{\rm p}}. \tag{17}$$

At the boundary of the cell interfaces $x_{\rm m\pm\frac{1}{2}}$ and $\rho_{p\rm n\pm\frac{1}{2}}$, a first order accurate scheme is used along the axial direction for the flux vectors $\mathbf{c}$ and $\mathbf{c}_{\rm p}$, and is approximated as [16, 24]

$$(\mathbf{c})_{\rm m+\frac{1}{2}} = (\mathbf{c}_m \qquad (\mathbf{c})_{\rm m-\frac{1}{2}} = (\mathbf{c})_{\rm m-1}, \tag{18}$$

$$(\mathbf{c}_{\rm p})_{\rm m,n+\frac{1}{2}} = (\mathbf{c}_{\rm p})_{\rm mn} \qquad (\mathbf{c}_{\rm p})_{\rm m,n-\frac{1}{2}} = (\mathbf{c}_{\rm p})_{\rm m,n-1}. \tag{19}$$

At the interior interfaces of the cells, a second order flux-limiting high resolution scheme is used and the approximations are given as [22, 16]

$$(\mathbf{c})_{\rm m+\frac{1}{2}} = (\mathbf{c})_{\rm m} + \frac{1}{2}\alpha(\varphi_{\rm m})((\mathbf{c})_{\rm m} - (\mathbf{c})_{\rm m-1}), \quad \varphi_{\rm m} = \frac{(\mathbf{c})_{\rm m+1} - (\mathbf{c})_{\rm m} + \psi}{(\mathbf{c})_{\rm m} - (\mathbf{c})_{\rm m-1} + \psi}, \tag{20}$$

$$(\mathbf{c}_{\rm p})_{\rm m,n+\frac{1}{2}} = (\mathbf{c}_{\rm p})_{\rm mn} + \frac{1}{2}\beta(\phi_{\rm mn})((\mathbf{c}_{\rm p})_{\rm mn} - (\mathbf{c}_{\rm p})_{\rm m,n-1}), \quad \phi_{\rm mn} = \frac{(\mathbf{c}_{\rm p})_{\rm m,n+1} - (\mathbf{c}_{\rm b})_{\rm mn} + \psi}{(\mathbf{c}_{\rm p})_{\rm mn} - (\mathbf{c}_{\rm p})_{\rm m,n-1} + \psi}. \tag{21}$$

To avoid having a division by zero in the above approximation in equations (20) and (21), ψ is chosen as a very small value, e.g. $\psi = 10^{-10}$. Furthermore, to preserve the local monotonicity of the technique, the flux-limiting functions α and β are taken as (c.f. [16])

$$\alpha(\varphi_{\rm m}) = \max\left(0, \min\left(2\varphi_{\rm m}, \min\left(\frac{1}{3} + \frac{2}{3}\varphi_{\rm m}, 2\right)\right)\right), \tag{22}$$

$$\beta(\phi_{\rm mn}) = \max\left(0, \min\left(2\phi_{\rm mn}, \min\left(\frac{1}{3} + \frac{2}{3}\phi_{\rm mn}, 2\right)\right)\right). \tag{23}$$

To obtain a second order accurate solution in time coordinate, which solves the expressions given in equations (15)-(23), a total variation diminishing Runge-Kutta second order scheme is applied [24]. We represent the right-hand-side of equations (15) and (16) by $\mathcal{A}(\mathbf{c}, \mathbf{c}_{\rm p}\,|_{\rho_{\rm p}=1})$ and $\mathcal{B}(\mathbf{c}_{\rm p})$ and apply the suggested scheme given below to update the stages of $\mathbf{c}$ and $\mathbf{c}_{\rm p}$

$$\mathbf{c}^{(1)} = \mathbf{c}^{\rm k} + \Delta\tau\mathcal{A}(\mathbf{c}^{\rm k}, \mathbf{c}_{\rm p}^{\rm k}\,|_{\rho_{\rm p}=1}), \quad \mathbf{c}^{\rm k+1} = \frac{1}{2}[\mathbf{c}^{\rm k} + \mathbf{c}^{(1)} + \Delta\tau\mathcal{A}(\mathbf{c}^{(1)}, \mathbf{c}_{\rm p}^{(1)}\,|_{\rho_{\rm p}=1})], \tag{24}$$

$$\mathbf{c}_{\rm p}^{(1)} = \mathbf{c}_{\rm p}^{\rm k} + \Delta\tau\mathcal{B}(\mathbf{c}_{\rm p}^{\rm k}), \quad \mathbf{c}_{\rm p}^{\rm k+1} = \frac{1}{2}[\mathbf{c}_{\rm p}^{\rm k} + \mathbf{c}_{\rm p}^{(1)} + \Delta\tau\mathcal{B}(\mathbf{c}_{\rm p}^{(1)})]. \tag{25}$$

Conventionally, $\mathbf{c}^{\rm k}$ and $\mathbf{c}_{\rm p}^{\rm k}$ represent the solutions at previous dimensionless time-step $\tau^{\rm k}$, while $\mathbf{c}^{\rm k+1}$ and $\mathbf{c}_{\rm p}^{\rm k+1}$ expresses the solutions at new time-step $\tau^{\rm k+1}$. The dimensionless time step $\Delta\tau$ is chosen by the Courant-Friedrichs-Lewy (CFL) condition given as

$$\Delta\tau \le \frac{1}{2}\min\left(\Delta x, \Delta x^2\min(Pe), \frac{\Delta\rho_{\rm p}^2}{\max(J_{\rm lmn}^{-1}\eta)}, \frac{\Delta\rho_{\rm p}}{2\max(J_{\rm lmn}^{-1}\eta)}\right). \tag{26}$$

The above algorithm was implemented in C language for mesh points of $60\times30\times20$ and executed using Intel processor of dual-core laptop computer with a RAM size of 8 gigabytes.

Table 1: Standard parameters used in the test problems.

Parameter	Symbol	Value
Henry's constant	H_1	1.0
Henry's constant	H_2	1.5
Langmuir factor	b_1	0.5
Langmuir factor	b_2	1.0
External porosity	ϵ	0.4
Internal porosity	ϵ_p	0.5
Peclet number	Pe	1500
Dimensionless constant	η	2
Dimensionless constant	ζ	50
Injected concentration	c_{inj}	1 mol/l
Time of injection	τ_{inj}	1.0

4 Results and discussion

The parameters used for the simulation of the results in this section falls within the range typically encountered in experimental studies of liquid chromatography [1]. The figures presented were plotted at the outlet of the column at the time the concentration exits the column, hence the plot of concentration against time and not the axial axis.

4.1 Effects of injected concentration size and time of injection

The first result shown in Figure 1(a) displays the effects of the size of the solute injected into the column on the output profile displayed at the outlet. The profile is seen to increase in direct proportion to the amount injected respectively. It can also be observed that the band widths are proportional to the size of the quantities injected into the column, which is an expected phenomenon. Figure 1(b) shows the

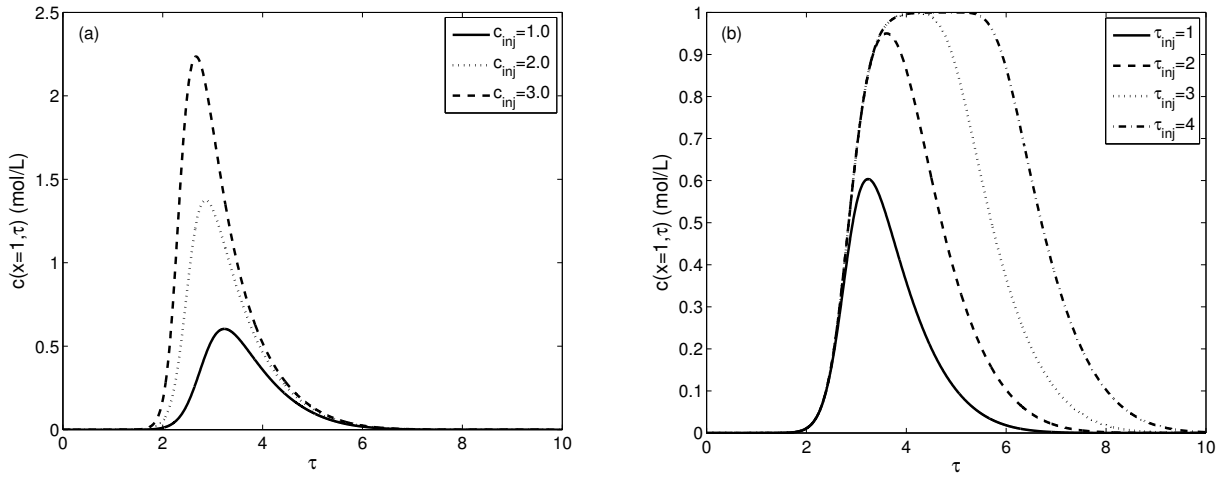

Figure 1: Effects of size of c_{inj} and τ_{inj}

effects of increasing the injection time, plotted at the end of the column. It can be seen that as the injection time is increased, the separation time is reduced which ultimately results to the profile being broader and this is seen to cause the eluent leaving the column at a much later time. It should be noted that the amount of injected concentration c_{inj} for this case is 1 mol/L, as can be seen from the figure.

4.2 Effects of the Langmuir factors

The results in Figure 2 show the effects of the Langmuir factors b_1, b_2 on the solute profiles. Other parameters used remain as given in Table 1 For increased Langmuir factors, the signature shape of the Langmuir isotherm profiles can be clearly observed. This gives sharper peak heights, a well visible

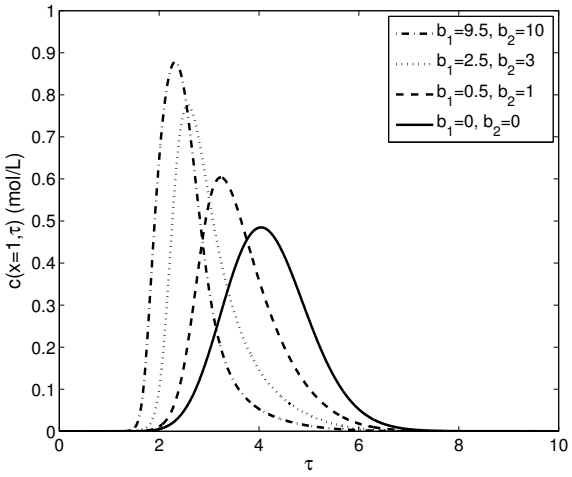

Figure 2: Effects of the Langmuir factors b_1, b_2

tailing to the right causing the profiles to be more diffusive.

4.3 Effects of kinetic parameters

Figure 3 give results of the effects of the kinetic parameters Pe and η on the elution profiles. The first result shown in Figure 3(a) shows that for increased value of Pe, a better profile with sharper peak height is achieved in a shorter time. Figure 3(b) displays the results for increasing values of η.

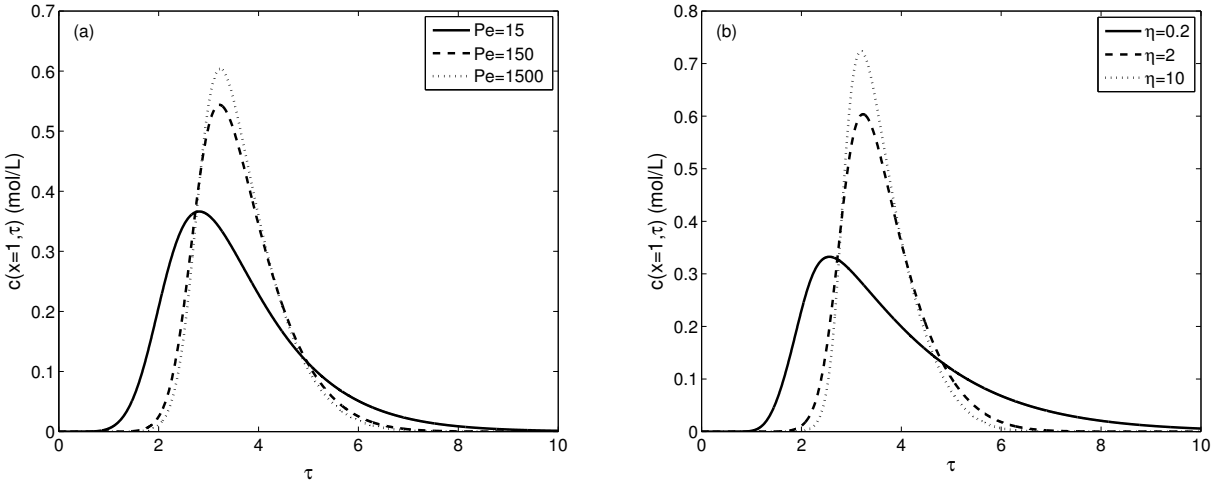

Figure 3: Effects of kinetic parameters Pe and η

Just like in the case of Pe, similar behavior can be observed on the elution profiles as the value of η is increased. In particular, it can be seen that for the smaller value of η, the concentration still has not exited the column at the maximum time plotted on the graph, that is at $\tau = 10$. The last result in

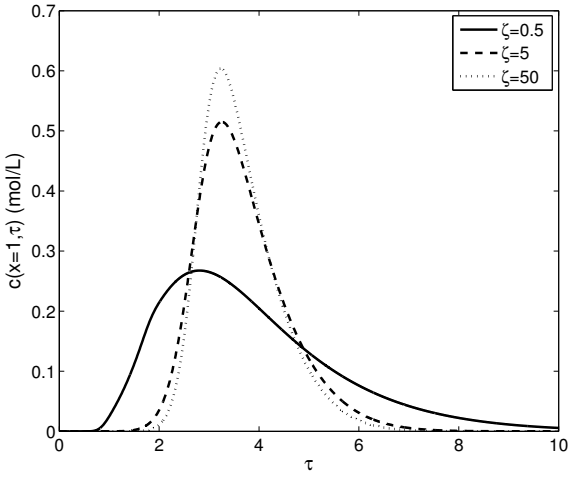

Figure 4: Effects of kinetic parameter ζ

this subsection is given in Figure 4. It shows that for increasing values of ζ, the elution profiles again behaves similar to the cases of both Pe and η. This shows that better column performance is achieved for increased kinetic parameters value.

4.4 Two components elution

Here, results of elution profiles of two mixed components are presented. Two results analyzing the effects of the Henry's constants H_{11}, H_{21}, both for component 1 and H_{12}, H_{22} both for component 2 and the Langmuir factors on the elution profiles are shown. The langmuir factors in this case are given as b_{11}, b_{21} both corresponding to component 1 and b_{12}, b_{22} both corresponding to component 2. The parameters given in Table 1 were used for the simulation of the results shown here for both components except where stated otherwise. For example, the values used in the simulation for η_1 and

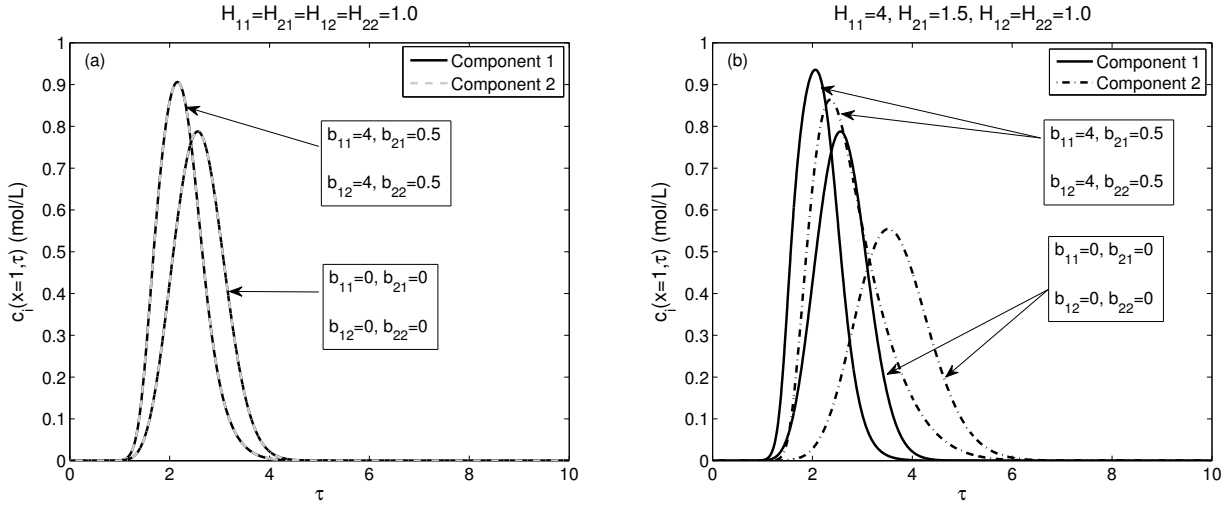

Figure 5: Two components elution showing effects of Henry's constants and Langmuir factors

η_2 is 1. Figure 5(a) shows two cases, the first case is for when the values of the Langmuir factors are taken as zero and the second case is when the values of the Langmuir factors are not zero. Also, there is a uniform value for the Henry's constant for the results obtained in Figure 5(a). In Figure 5(b), the values of the Henry's constant are assigned such that there is separation of components 1 and 2. The

results show that a better separation is achieved in the case where the values of the Langmuir factors are not zero. Hence, the presence of the Langmuir factors give sharper peak heights and enhance better separation of the elution components.

5 Conclusion

In this work, a one-dimensional general rate model of liquid chromatography was used to simulate the process under isothermal operating condition considering the nonlinear bi-Langmuir isotherm. The governing model equations consist of a system of PDE's coupled with algebraic isothermal expressions. Due to the nonlinear nature of the equations, caused by the application of the nonlinear bi-Langmuir isotherm, numerical approximation of the solutions of the model equations were sought. A second order semi-discrete finite volume scheme was implemented to obtain the solutions. Various test problems involving one- and two-component mixtures were carried out. The results show that the presence of the Langmuir factors provided better elution profiles and better separation for mixed components. Moreover, results show that the suggested numerical scheme provided moderate predictions of and non-oscillating solutions. These results can further help in the improvement of liquid chromatographic processes.

References

[1] Guiochon, G., Felinger, A., Shirazi, D.G. and Katti, A.M. (2206). Fundamentals of preparative and nonlinear chromatography, 2nd ed. ELsevier Academic press, New York.

[2] Bérot, S., Compoint, J.P., Larré, C., Malabat, C. and Guéguen, J. (2005). Large scale purification of rapeseed proteins (Brassica napus L.). Journal of Chromatography B 818, 35-42.

[3] Hofmann, M. (2003). Use of ultrasound to monitor the packing of large-scale columns, the monitoring of media compression and the passage of molecules, such as monoclonal antibodies, through the column bed during chromatography. Journal of Chromatography A 989, 79-9.

[4] Stickel, J.J. and Fotopoulos, A. (2001). Pressure-flow relationships for packed beds of compressible chromatography media at laboratory and production scale. Biotechnology Progress 17, 744-751.

[5] Guiochon, G. (2002). Preparative liquid chromatography. Journal of Chromatography A 965, 129-161.

[6] Bellot, J.C. and Condoretm J.S. (1991). Liquid Chromatography Modelling : A Review. Process Biochemistry 26, 363-376.

[7] Guiochon, G. and Lin, B. (2003). Modeling for preparative chromatography, Academic Press, San Diego (CA).

[8] Carta, G. (1988). Exact analytical solution of a mathematical model for chromatographic operations. Chemical Engineering Science 43, 2877-2883.

[9] Ruthven, D.M. (1984). Principles of adsorption and adsorption processes. Wiley-Interscience, New York.

[10] Crank, J. (1975). The mathematics of diffusion, 2nd ed. Clarendon Press, Oxford.

[11] Gu, T. (1995). Mathematical Modeling and Scale-Up of Liquid Chromatography. Springer, Berlin-New York.

[12] Qamar, S., Perveen, S., Seidel-Morgenstern, A. (2016). Numerical approximation of a two-dimensional nonlinear and nonequilibrium model of reactive chromatography. Industrial & Engineering Chemistry Research 55, 9003-9014.

[13] Qamar, S., Uche, D.U., Khan,F.U. and Seidel-Morgenstern, A. (2017). Analysis of linear two-dimensional general rate model for chromatographic columns of cylindrical geometry. Journal of Chromatography A 1496, 92-104.

[14] Rice, R.G. and Do, D.D. (1995). Applied mathematics and modeling for chemical engineers. Wiley-Interscience, New York.

[15] Qamar, S., Abbasi, J.N., Javeed, S. and Seidel-Morgenstern, A. (2014). Analytical solutions and moment analysis of general rate model for linear liquid chromatography. Chemical Engineering Science 107, 192-205.

[16] Javeed, S., Qamar, S., Seidel-Morgenstern, A. and Warnecke, G. (2011). Efficient and accurate numerical simulation of nonlinear chromatographic processes. Journal of Computers & Chemical Engineering 35, 2294-2305.

[17] David, U.U., Qamar, S. and Seidel-Morgenstern, A. (2018). Analytical and numerical solutions of two-dimensional general rate models for liquid chromatographic columns packed with core-shell particles. Chemical Engineering Research & Design 130, 295-320.

[18] Ahmad, A.G., Okechi, N.F., Uche, U.D. and Salaudeen, A.O. (2023). Numerical Simulation of Nonlinear and Non-Isothermal Liquid Chromatography for Studying Thermal Variations in Columns Packed with Core-Shell Particles. Journal of the Nigerian Society of Physical Sciences 5, 1350.

[19] Uche, U.D., Uche, M., Okafor F. and Utalor, K. (2022). Modeling and simulation of isothermal reactive liquid chromatography for two component elution-effects of core-shell particles. International Journal of Mathematical Sciences and Optimization: Theory and Applications 8(1), 117-128.

[20] Uche, U.D., Uche, M. and Okafor, F. (2021). Investigating the Effects of Core-Shell Particles on Non-Isothermal Reactive Liquid Chromatography. Journal of the Nigerian Mathematical Society 40, 97-128.

[21] Uche, U.D., Qamar, S. and Seidel-Morgenstern, A. (2020). Numerical approximation of a non-isothermal two-dimensional general rate model of reactive liquid chromatography. International Journal of Chemical Kinetics 52, 134–155.

[22] Koren, B. (1993). A robust upwind discretization method for advection, diffusion and source terms. In C. B. Vreugdenhil, B. Koren, editors, Numerical Methods for Advection-Diffusion Problems, Volume 45 of Notes on Numerical Fluid Mechanics, chapter 5, pages 117-138, Vieweg Verlag, Braunschweig.

[23] Lieres, E.V. and Andersson, J. (2010). A fast and accurate solver for the general rate model of column liquid chromatography. Computers & Chemical Engineering 34, 1180-1191.

[24] Cockburn, B. and Shu, C.-W. (1989). TVB Runge-Kutta local projection discontinuous Galerkin finite element method for conservation laws II, Gerneral framework. Mathematics of Computation 52, 411-435.